Intrinsic defects in perpendicularly magnetized multilayer thin films and nanostructures

Justin M. Shaw,[1] Miles Olsen,[1,2] June W. Lau,[3] Michael L. Schneider,[2] T. J. Silva,[1] Olav Hellwig,[4] Elizabeth Dobisz,[4] and Bruce D. Terris[4]

[1]*National Institute of Standards and Technology, Boulder, Colorado 80305, USA*

[2]*University of Montana, Missoula, Montana 59812, USA*

[3]*National Institute of Standards and Technology, Gaithersburg, Maryland 20899, USA*

[4]*Hitachi Global Storage Technologies, San Jose, California 95135, USA*

(Received 4 August 2010; revised manuscript received 5 October 2010; published 26 October 2010)

Intrinsic magnetic defects in perpendicularly magnetized nanostructures reduce the predictability of device and developing recording technologies. In addition to a distribution of local anisotropy fields, we show that such defects also exhibit variations in local anisotropy axes. The magnetic defects are identified by the application of in-plane and out-of-plane magnetic fields and magnetic force microscopy imaging. Those defects that control magnetization reversal in arrays of patterned Co/Pd multilayers are highly dependent on applied field orientation. The symmetry of the defects with respect to the applied field direction indicates that the anisotropy consists of a canted axis, deviating from the surface normal. Micromagnetic simulations confirm that variations in anisotropy axis can cause a significant change in reversal field depending on the location and orientation of the defects, consistent with experimental results.

DOI: 10.1103/PhysRevB.82.144437 PACS number(s): 75.70.−i, 75.75.−c, 75.78.Cd, 75.60.Jk

One critical barrier to the implementation of perpendicularly magnetized nanostructures in bit patterned media (BPM) (Refs. 1–6) and spintronic technologies[7,8] is the control of anisotropy variations in the magnetic material. Such variations manifest themselves as significant switching field distributions (SFDs) or high-frequency properties that vary from nanostructure to nanostructure, which decreases predictability of bit or device performance.[9–11] Hence, intrinsic anisotropy variation must be minimized in addition to extrinsic magnetic defects such as edge damage,[12] size variations, and lithographic defects.[13] In addition, the nature of the intrinsic magnetic defects that cause anisotropy distributions must be understood in order to facilitate more accurate and realistic models. The typical method to simulate intrinsic magnetic defects is to treat them as a distribution of local anisotropy fields.[9,14] However, an important property is ignored in such models: the anisotropy can also have a distribution of axes instead of, or in addition to, a distribution in anisotropy field magnitude. This can have significant consequences in BPM, for example, if some variation in the field direction is provided by the write head. In other words, the critical reversal field is dominated by defects, and the defects responsible for reversal may depend on the orientation of the applied field.

Much of the motivation for this work is rooted in the reversal process that occurs in perpendicularly magnetized nanostructure such as Co/Pd multilayer systems, where the system is highly exchange coupled. Both experimental evidence and micromagnetic simulations indicate that a small volume with dimensions (on the order of the exchange length) nucleates and is subsequently followed by rapid domain-wall movement until the entire nanostructures has reversed.[12,15–17] Because the depinning fields are much lower than the nucleation fields, the nucleation volume cannot be reversed independently from the rest of the nanostructure when using a static out-of-plane field in such highly exchange coupled systems. As a result, defects that largely control the switching properties of nanostructures cannot be easily isolated and studied directly. Throughout this article, we use the term "defect" to indicate a nucleation volume that has a lower value than the average nucleation field value or activation energy.

To date, two methods have been demonstrated to isolate magnetic defects in exchange coupled materials with a large perpendicular anisotropy. One relies on rapid Joule heating of the sample near the Curie temperature with a current pulse such that regions with the lowest energy barrier reverse through magnetostatic interactions.[18] The second method, employed in this study, makes use of an in-plane field to lower the energy barrier and induce reversal of defect regions.[16] By applying this technique in a systematic angular-dependent study, we show that intrinsic magnetic defects have a distribution of magnetic axes. This result has significant implications in future studies and modeling of magnetic defects, which should include a distribution of axes in addition to possible fluctuations in the magnitude of the anisotropy.

We focus on a patterned Co/Pd multilayer sample. The Co/Pd multilayer was dc-magnetron sputter deposited on a prepatterned Si(001) substrate with the following structure: Ta(1.5 nm)/Pd(3 nm)[Co(0.45 nm)/Pd(0.9 nm)] $\times 8$/Pd(1.1 nm). The Ta seed layer was used to ensure the microstructure was highly (111) textured.[11] The pillar structures on the prepatterned silicon substrates were formed by electron-beam lithography and a reactive ion etch as outlined in Ref. 19. The use of the so-called prepatterned fabrication method was used to minimize (or avoid) the effect of edge damage on reversal properties.[12]

The magnetic configuration and domain structure were identified using magnetic force microscopy (MFM) at room temperature. Because the magnetic configuration can be influenced by the stray field of the cantilever tip, we exclusively used tips with a moment below 3×10^{-17} A m^2. By repeated measurements of the same location, we confirmed that these tips have a minimal impact on domain-wall location or motion.

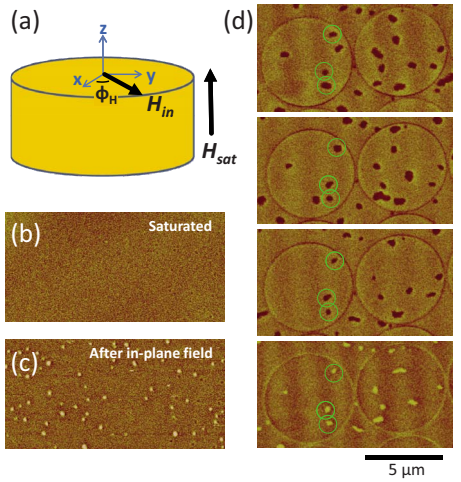

FIG. 1. (Color online) (a) Schematic showing the definitions and orientation of the applied magnetic field. MFM images of a region in a thin-film sample (b) before and (c) after the application of a critical in-plane field. (d) A series of repeated MFM measurements on 5 μm structures showing the repeatability of the location of the nucleated sites. The bottom image had the applied field polarities reverse to show the independence of the nucleation site positions on the saturation field direction.

The magnetic defects are identified by the following procedure. The samples are first saturated by applying a large, out-of-plane saturation field $\mu_0 H_{sat} = \pm 1.3$ T (significantly larger than the coercive field) as depicted in Fig. 1(a). The absence of any features in MFM images—an example of which is shown in Fig. 1(b)—also verifies that the sample is saturated. Magnetic defects have previously been shown to nucleate as a result of the application of a critical in-plane field.[16] Such an in-plane field $\mu_0 H_{in} = 0.65$ T at angle ϕ_H [defined in Fig. 1(a)] is applied until small regions are observed to undergo reversal as shown in the remanent MFM image in Fig. 1(c). The magnetic defects are likely much smaller than the 50–200 nm domains observed in the MFM image. The magnetostatic and exchange energies likely increase the size of these domains once they are nucleated at the defect site. In other words, competition of the magnetostatic energy with the domain-wall energy sets the size of the resulting domains, which can be significantly larger than the defect that originally triggers the nucleation. As the in-plane field is further increased, more defect sites are created since a larger number of energy barriers can be overcome. Again, it is important to point out that such defects cannot be studied through the application of an out-of-plane static field since the nucleation field is significantly higher than the depinning field. The consequence of this condition is that the reversal process is one of nucleation followed by rapid domain-wall movement.[12,15–17]

Up until this point, we have made the assumption that the small nucleated regions are magnetic defects, versus a random temporal event. In order to confirm this assumption, we repeat the measurement several times at the same location in the sample, saturating the sample each time. The series of images in Fig. 1(d) show that the locations of the reversed regions are highly repeatable, and therefore, a result of a local property or defect of the material and not a random temporal event. The repeatability is observed in thin films as well as nanostructures as small as 50 nm in diameter (not shown). In nanostructures smaller than 100 nm, however, the structures are single domain and, as a result, the entire nanostructure reverses. However, the repeatability is still demonstrated since the same nanostructures undergo reversal when the measurement is repeated. The smaller structures also require a slightly greater in-plane field before reversal occurs, likely due to shape and size effects.

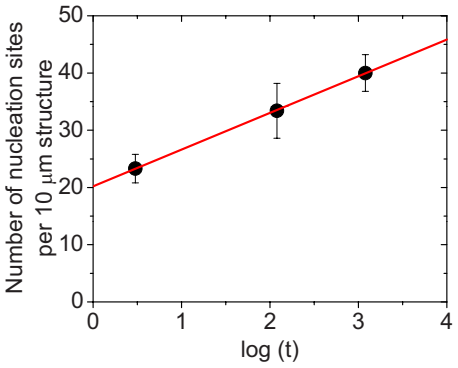

FIG. 2. (Color online) Number of nucleated sites in a 10-μm-diameter structure as a function of the time the in-plane field was applied. The time has been normalized to 1 s.

A recent study that relied on transmission x-ray microscopy measurements and first-order reversal curve analyses showed that saturation fields for out-of-plane anisotropy materials are significantly higher than the coercive fields.[20] In that study, extremely small regions (not observable with MFM) remain unsaturated even when large out-of-plane fields are applied. If such unsaturated sites remain, then it is possible that the defect sites we identify are instead unsaturated sites undergoing domain growth with the applied fields until they can be detected with MFM. In order to exclude that effect, we repeat the process using a saturation field with the opposite external field polarity, which is included in Fig. 1(d). This image shows the majority of the reversed regions are independent of the saturation field polarity, confirming that the sample is fully saturated with the $\mu_0 H_{sat} = 1.3$ T used in this study. We note that those regions that are not present in *every* measurement are still observed to repeatedly reverse in several measurements, indicating they have a probability of occurrence. This indicates that these regions have a higher energy barrier relative to the regions observed to reverse 100% of the time.

We have established through the repeatability of reversed regions and independence of the field polarity that the nucleated regions are due to a defect in the material. However, if the energy barrier is overcome by a thermal event, then the number of reversed regions should increase as the time that the in-plane field is applied is increased. Indeed, Fig. 2 shows the time dependence of the number of reversed sites in several 10 μm structures with an in-plane field of $\mu_0 H_{in} = 0.65$ T. These data show a logarithmic time dependence across almost three decades. Under the assumption of a distribution of energy barriers and dipole interactions, thermal relaxation of the material is predicted to be logarithmic in

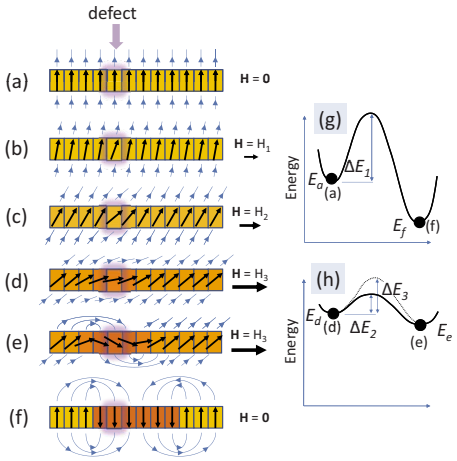

FIG. 3. (Color online) Schematic, cross-sectional illustration of the process that occurs during the formation of a nucleated region when applying an in-plane field. The defect (modified anisotropy) region is the highlighted segment. [(a) and (f)] Magnetic configuration in the remnant state before and after the nucleation event, respectively. [(b)–(e)] Magnetization as an in-plane field is gradually applied. (g) Energy state and energy barrier between the magnetic configuration depicted in (a) and (f). (h) Energy state and energy barrier between the magnetic configurations depicted in (d) and (e). The dotted line in (e) represents the energy barrier for a defect-free region.

time.[21–24] These data further support the case that the nucleation sites identified in this work are defects with a reduced energy barrier and require a thermal "kick" to overcome an energy barrier for reversal to occur.

The above evidence suggests that the nucleation sites we identified reverse via an in-plane applied field through the mechanism depicted in Fig. 3. Here, we schematically show a cross-section view of a perpendicularly magnetized thin film that is divided into sections that can be considered grains or volumes with dimensions on the order of the exchange length. Initially, the film is saturated and in a remanent state at energy E_a [Fig. 3(a)]. The magnetostatic energy, however, favors the formation of a domain as depicted in Fig. 3(f), which provides some flux closure. This would result in a reduction in the energy to E_f (assuming the domain-wall energy is smaller than the change in magnetostatic energy.) However, the energy barrier ΔE_1 is too large to be overcome at room temperature with no external field applied, and therefore remains in a saturated state. As an in-plane field is applied [Figs. 3(b) and 3(c)], the magnetic moments begin to rotate in the direction of the field. At a defect region (depicted as the highlighted region in Fig. 3), the magnetization may respond differently relative to the rest of the film due to, for example, a modified anisotropy. As the external field is increased to H_3, the energy barrier of the defect region ΔE_2 becomes small enough such that there is a high probability of a thermal fluctuation can overcoming the energy barrier. This is driven by the reduction in magnetostatic energy that occurs when the defect region reverses. This process can occur at any location in the film regardless of the presence of a defect. However, the energy barrier for reversal of a defect-free region ΔE_3 will be significantly larger, decreasing the likelihood that a thermal fluctuation can overcome the barrier.

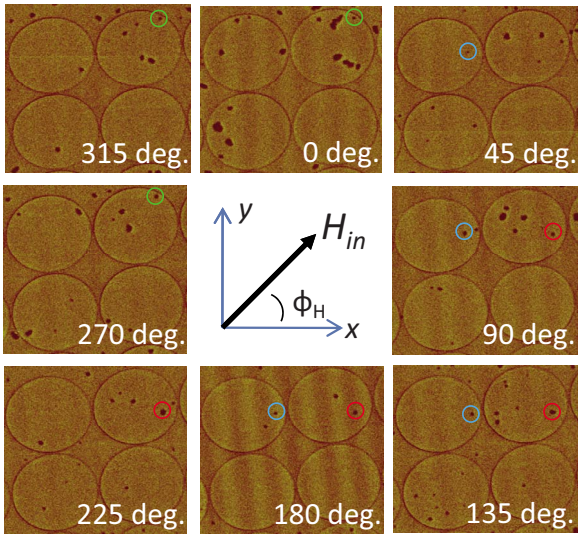

FIG. 4. (Color online) A series of MFM images taken on 5-μm-diameter structures for different values of in-plane field angle.

We now show that these defects are not only simply regions of reduced anisotropy but also exhibit a more complicated behavior that includes a deviation in anisotropy axis. Figure 4 shows a series of remanent MFM images of several 5-μm-diameter structures in which the in-plane angle ϕ_H was varied. As ϕ_H is changed, the locations of the nucleated regions change indicating that different defects undergo reversal. Again, the repeatability of the defect locations was confirmed by multiple measurements at the same value of ϕ_H (not shown). As shown in Fig. 4, most defects are present at a single angle. However, some defects are present at two or more values of ϕ_H, but they always occur within a certain angular range centered along a single direction (such as the defects circled in Fig. 4).

One conclusion is that these defects have axes associated with them that deviate from the surface normal and are not solely regions of *reduced* anisotropy. Of great importance is the fact that the in-plane symmetry of the defects is unidirectional and not uniaxial. This suggests that the defects consist of a canted perpendicular anisotropy versus an additional in-plane uniaxial anisotropy component. This has strong implications in the understanding of such defects since, for example, a microstructural defect (misaligned grain in a highly textured material) may introduce a magnetocrystalline anisotropy with a canted axis instead of, or in addition to, a modification of the magnitude of the anisotropy. Recent simulations that assume a distribution of anisotropy fields show a minimum in the SFDs when the applied field angle is 45°.[15] That work suggests that the effects of anisotropy distributions may be partially mitigated by switching the bit with an applied field at an optimal angle. However, the optimal angle may be altered if a distribution of axes is also taken into consideration.

With this in mind, we now address the connection between the defects identified by the application of an in-plane

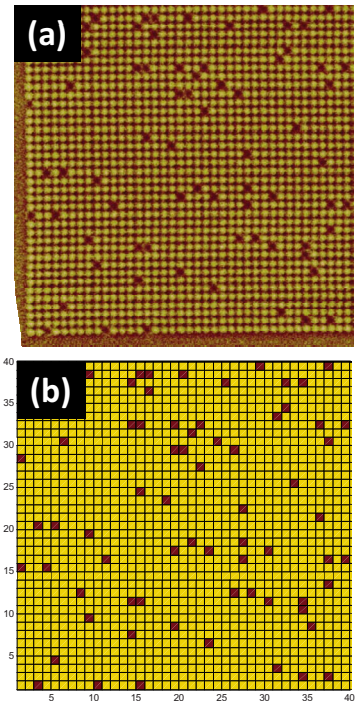

FIG. 5. (Color online) (a) An MFM image and (b) its converted binary matrix of an array of 200–nm-diameter nanostructures.

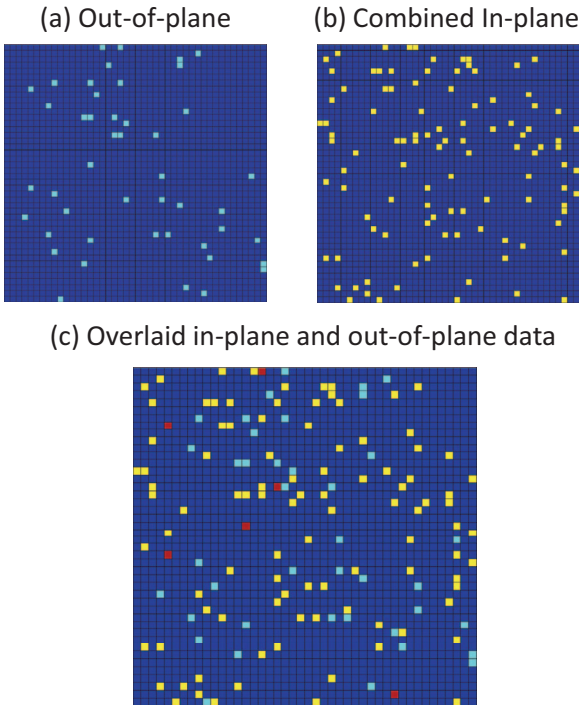

FIG. 6. (Color) The composite matrices for the (a) out-of-plane and (b) in-plane applied fields. The data are overlaid in (c). Red indicates cells that have undergone reversal in both the out-of-plane and in-plane cases.

field and out-of-plane reversal fields in nanostructures that lead to SFDs. In other words, we need to answer the question: are the defects identified with an in-plane field the same defects responsible for the "easy switchers" in an array of nanostructures? We will focus our attention on an array of 200-nm-diameter nanostructures since they are small enough to obtain sufficient statistics, yet they are also larger than the nucleation sites identified in the MFM images. However, we studied structures as small as 50 nm in diameter and they exhibit similar behavior.

Figure 5(a) shows a remanent MFM image of an array consisting of 200-nm-diameter structures following the application of an out-of-plane field $\mu_0 H_{out}$=+0.68 T. These samples were initially saturated with an out-of-plane saturation field of $\mu_0 H_{sat}$=−1.3 T. At the application of H_{out}, only a few nanostructures reverse, which we identify as the nanostructures with the lowest reversal fields, the so-called easy switchers.

For the analysis here, the MFM images are converted into a digital binary matrix through the use of a custom image analysis software. Since the corner of the array is always in view, thereby providing a fiducial marker, the conversion to a binary matrix allows each nanostructure to be uniquely identified throughout the study. Figure 5 shows an example of a binary matrix and the corresponding MFM image from which it was created

As a first step, we identify the easy switchers by the application of a 0.68 T out-of-plane field and repeat this measurements five times (resaturating the sample after each application of H_{out}) to verify repeatability. This process ensures that we are identifying the nanostructures with the lowest reversal fields in the array since less than 5% of the structures reverse at this field. Again, we repeat the measurements with the opposite polarity of H_{sat} and H_{out} to ensure that sufficient saturation field was used. Figure 6(a) shows the matrix with the combined data from all six measurements. Here, only those nanostructures that repeatedly reverse for all six measurements are included, which accounts for approximately 58% of the total number of nanostructures that underwent a reversal event. However, the results of our analysis do not change if the constraints on the allowed reversal events are exclusive or inclusive of the reversal events in a series of repeated measurements.

Next, we identify nanostructures that contain a defect with the lowest energy barriers through the application of an *in-plane* field. The array was first saturated with an out-of-plane field $\mu_0 H_{sat}$=−1.3 T prior to the application of an in-plane field $\mu_0 H_{in}$=+0.9 T. Since the 200 nm structures are capable of supporting multidomain states, we then apply an additional out-of-plane "fixing" field $\mu_0 H$=+0.3 T. This field is large enough to completely reverse a nanostructure that already contains a nucleated region but is small enough that it will not reverse nanostructures that are fully saturated. Similar to the defect sites in larger structures, different nanostructures reversed depending on the in-plane field direction ϕ_H. As a result, we must identify the nanostructures that switch at all values of ϕ_H. We therefore perform measurements with $\mu_0 H_{in}$=+0.9 T applied at increments of 45° for a full 360° rotation. A 45° increment in ϕ_H was small enough due to the fact that the majority of the reversed nanostructures are present within an angular range larger than 45° (i.e., present in multiple adjacent values of ϕ_H).

The composite matrix from all the in-plane data is shown in Fig. 6(b). At a given value of ϕ_H, the measurement was

repeated at least twice, which always contains at least one measurement with the opposite polarities of the fields. As with the out-of-plane data, only those nanostructures that were found to reverse in all of the measurements (at a given ϕ_H) were included. The matrices for each value of ϕ_H were then combined into the composite matrix of Fig. 6(b).

Figure 6(c) shows an overlay of the composite matrices for both the out-of-plane and in-plane data. Surprisingly, there is very little correlation between the nanostructures that contain a defect identified with an in-plane field and those identified as easy switchers from an out-of-plane field. This result indicates that the defects identified with an in-plane field are rarely the same defects responsible for nucleating reversal with an out-of-plane field.

To gain further insight into the mechanism giving rise to these results, we performed micromagnetic simulations using the object-orientated micromagnetic framework (OOMMF) simulation package, including edge-error corrections.[25] For these simulations, we used the following materials parameters, which are practical values for this material:[12] magnetization $M_s=5\times10^5$ A/m, out-of-plane uniaxial anisotropy energy $K=8\times10^5$ J/m^3, damping constant $\alpha=0.1$, and an exchange stiffness constant $A=1\times10^{-11}$ J/m. The thickness of the material was set at 12 nm with a cell size of $1\times1\times3$ nm^3. Unless otherwise stated, the defects are modeled as a 10-nm-diameter region of modified anisotropy to simulate a defect grain or region and extends through the entire thickness of the material to simulate a columnar grain structure. Simulations were performed on an isolated 50-nm-diameter nanostructure with the applied field offset by 3° from the surface normal to break the symmetry. We note that no thermal fields were used in these simulations, and therefore simulate the system at $T\approx0$ K. The typical consequence of this condition is that the reversal field is significantly higher than in experiment where the system is thermally assisted.

We first consider the case where the defect consists of a reduction in the magnitude of the anisotropy. Figures 7(a)–7(c) show the dependence of the switching field H_{sf} on the magnitude of the defect anisotropy, size, and location of the defect in the nanostructure, respectively. The results show a strong dependence of the switching field on the magnitude of the defect anisotropy and the size. However, only a small effect on the position of the defect is observed, which has the slight reduction in H_{sf} as the defect nears the edge of the nanostructure.

Since we show that the defects appear to result from a variation in anisotropy axes instead of (or in addition to) a change in the magnitude of the anisotropy, we also simulated defects for which the anisotropy axis is canted with respect to the surface normal. In this case, we keep the anisotropy constant and only vary the anisotropy axis. We define the anisotropy axis in polar coordinates as depicted in Fig. 8(a). In this convention, $\theta_{def}=0°$ corresponds to an out-of-plane anisotropy axis and $\theta_{def}=90°$ corresponds to an in-plane anisotropy axis. For simplicity, we focus on the three cases shown in Fig. 8(b). The switching field was simulated as the defect polar angle θ_{def} is rotated from out-of-plane to in-plane along the azimuthal angle ϕ_{def}, the projection onto the x-y plane of which is shown as the arrow in Fig. 8(b). The

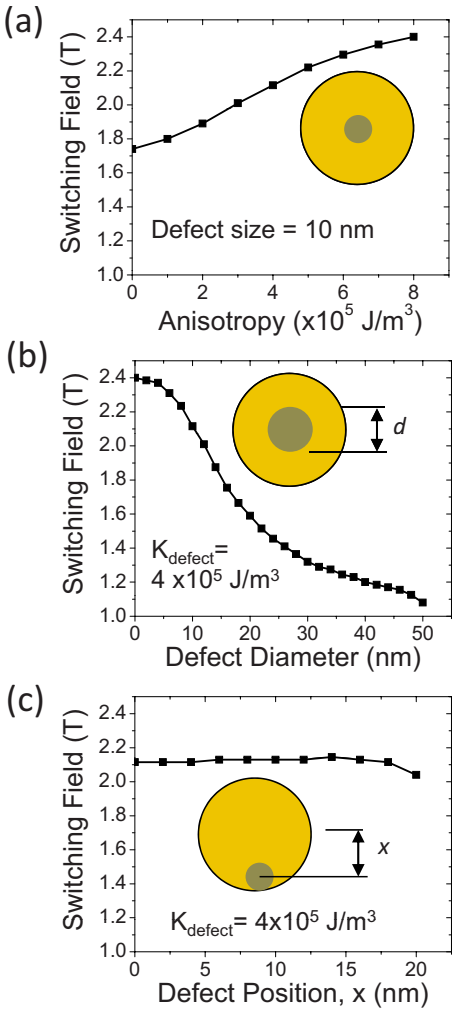

FIG. 7. (Color online) Micromagnetic simulations of the switching field in a 50 nm structure that contains a defect with a reduced value of anisotropy as a function of the (a) defect anisotropy, (b) defect size, and (c) defect position.

results of the simulations are summarized in Fig. 8(c). Significant differences of the dependence of the switching field on anisotropy angle were observed for the three cases in question. These simulation results suggest that both location and anisotropy-axis orientation are equally important in determining the reversal field. Indeed, the dependence of switching field on the range of values considered for θ_{def} is comparable to those obtained from defects modeled strictly as variations in anisotropy magnitude (Fig. 7). As a result, both models could presumably account for the observed SFDs in nanostructure. However, because of the broken symmetry of the in-plane data in Fig. 4, a distribution of anisotropy axes must (at least in part) be a property of the defects.

Taking the same three cases of defect position and axes, we then simulated the switching field with an in-plane field. As with the out-of-plane simulations, the field was offset 3° ($\theta_H=93°$) to break the symmetry and facilitate identification of a switching event. Figure 9 shows the result of the in-plane simulations. For comparison, out-of-plane switching data are also included as the closed black symbols. The switching field behavior varied considerably with the differ-

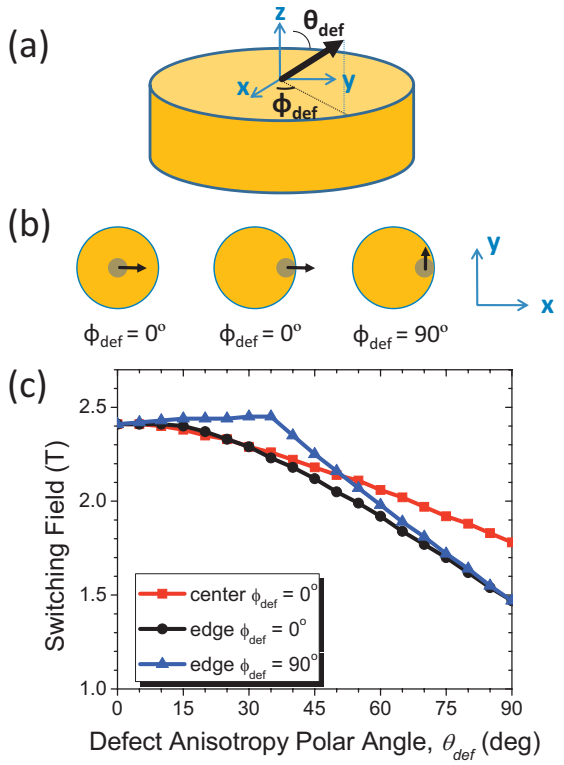

FIG. 8. (Color) (a) Polar coordinates used to define the defect anisotropy axis. (b) Three defect locations and anisotropy axis configurations used in the simulations. (c) Micromagnetic simulations of the out-of-plane switching filed as a function of the polar angle of a canted defect anisotropy axis for the three cases shown in (b).

ent values of the in-plane angle ϕ_H. In fact, the minimum switching field occurs along only one direction, consistent with the unidirectional in-plane symmetry of the experimental data. Overall, the in-plane switching field is seen to depend on both the position and orientation of the defect relative to the applied in-plane field direction. The variation in the in-plane switching field with ϕ_H is consistent with the experimental data for nucleation sites in larger structures as well as the in-plane switching data in smaller single-domain structures. A minimum in switching field exists at $\phi_{def} \approx 15° - 20°$, which indicates that defects that have a canted axis within a narrow range of angle may be most influential in nucleating reversal. However, simulations on all configurations of defect anisotropy would need to be performed in order to confirm such a conclusion.

Comparison of the simulated results for the in-plane and out-of-plane switching data shows that these quantities can have very different values, as well as angular dependencies. This is an important result since these simulations are consistent with the lack of correlation between the defects experimentally identified with an in-plane field and the easy switchers identified with an out-of-plane field. To serve as an example, Fig. 9(d) shows that below ≈35°, the nanostructure will not be considered an easy switcher with an out-of-plane field since there is no reduction (but actually a small increase) in the switching field. However, with an in-plane field applied along the ϕ_H=270° direction, the nanostructure will reverse at a considerably reduced field. Thus, we have established a mechanism in which the defect responsible for nucleating reversal depends on the applied field orientation.

The above evidence suggests that analysis and modeling of such defects should consider a variation in the anisotropy axis in addition to a variation in anisotropy magnitude to better describe realistic systems. The physical origin of the defects identified in this work are still uncertain, although some evidence indicates that misaligned grains and/or localized variation in the multilayer thickness contribute.[10,11] Future work to quantify and separate the variation in anisotropy axis and magnitude would further improve the understanding and ability to model such material systems. Of great importance to technology, however, is how the defects identified in this study will affect the switching process in the high speed (<1 ns) regime where both spintronics devices and BPM will likely operate. Such measurements provide many opportunities for future work and experiments.

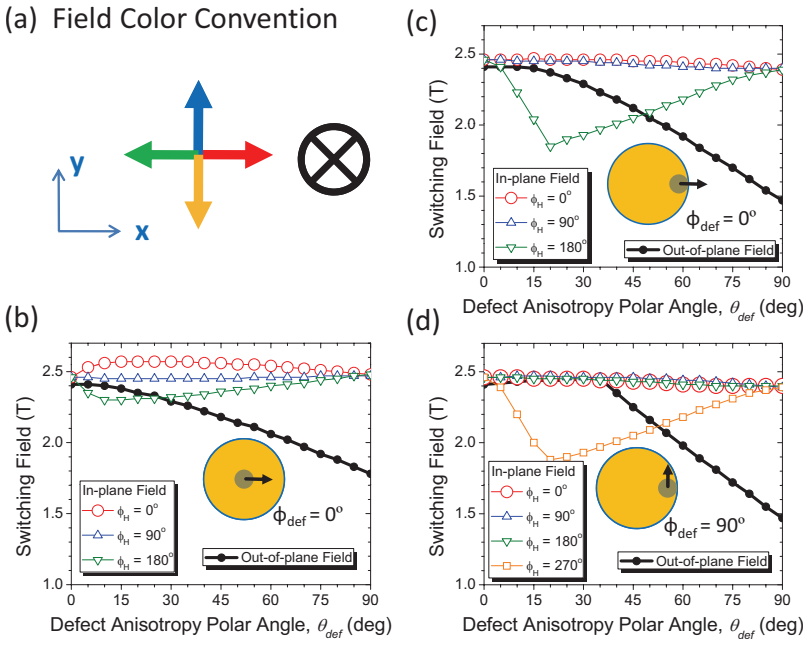

FIG. 9. (Color) (a) Summary of the color convention used to distinguish the applied field directions used. [(b)–(d)] Micromagnetic simulations of in-plane switching fields as a function of the polar angle of a canted defect anisotropy axis for the three cases. For comparison, the simulated out-of-plane switching field data is included as the black data points.

Finally, realistic nanostructures will likely contain contributions from both intrinsic defects, as well as extrinsic defects such as edge damage[12] and roughness. Both of these factors have been shown to have significant influence on the reversal properties in perpendicularly magnetized nanostructures. The current work focuses on the behavior and properties of intrinsic defects. The use of the prepatterned fabrication process was intentionally used to minimize the influence of extrinsic edge defects on the system. However, for most applications the prepatterned process is not a practical approach. As a result, models need to be developed and future experiments need to be designed that include (and correlate) intrinsic defects and extrinsic contributions.

In summary, magnetic defects with a modified local anisotropy can be identified by the application of an in-plane field and subsequent imaging with MFM. In-plane angular-dependent measurements indicate that the anisotropy axis of magnetic defects in Co/Pd multilayers is locally canted. Measurements on smaller structures show that defects identified with an in-plane magnetic field do not correlate with the easy switchers identified with an out-of-plane field. Micromagnetic simulations show the reversal field is highly dependent on the applied field direction, the position of the defect within the structure, and the defect anisotropy axis orientation. The simulations also predict very different trends in the switching properties when an in-plane or out-of-plane field is used, consistent with the experimental results.

The authors are grateful to Hans Nembach, Robert McMichael, Stephen Russek, and Tom Thomson for valuable discussions. This work was partially supported by the National Institute of Standards and Technology's Innovation in Measurement Science program.

[1] B. D. Terris, J. Magn. Magn. Mater. **321**, 512 (2009).
[2] S. J. Greaves, Y. Kanai, and H. Muraoka, IEEE Trans. Magn. **44**, 3430 (2008).
[3] M. Abes, M. V. Rastei, J. Venuat, A. Carvalho, S. Boukari, E. Beaurepaire, P. Panissod, A. Dinia, J. P. Bucher, and V. Pierron-Bohnes, J. Appl. Phys. **105**, 113916 (2009).
[4] R. Sbiaa, C. Z. Hua, S. N. Piramanayagam, R. Law, K. O. Aung, and N. Thiyagarajah, J. Appl. Phys. **106**, 023906 (2009).
[5] S. Okamoto, N. Kikuchi, T. Kato, O. Kitakami, K. Mitsuzuka, T. Shimatsu, H. Muraoka, H. Aoi, and J. C. Lodder, J. Magn. Magn. Mater. **320**, 2874 (2008).
[6] T. Hauet, E. Dobisz, S. Florez, J. Park, B. Lengsfield, B. D. Terris, and O. Hellwig, Appl. Phys. Lett. **95**, 262504 (2009).
[7] S. Mangin, D. Ravelosona, J. A. Katine, M. J. Carey, B. D. Terris, and E. E. Fullerton, Nature Mater. **5**, 210 (2006).
[8] W. H. Rippard, A. M. Deac, M. R. Pufall, J. M. Shaw, M. W. Keller, S. E. Russek, G. E. W. Bauer, and C. Serpico, Phys. Rev. B **81**, 014426 (2010).
[9] T. Thomson, G. Hu, and B. D. Terris, Phys. Rev. Lett. **96**, 257204 (2006).
[10] J. W. Lau, R. D. McMichael, S. H. Chung, J. O. Rantschler, V. Parekh, and D. Litvinov, Appl. Phys. Lett. **92**, 012506 (2008).
[11] J. M. Shaw, H. T. Nembach, T. J. Silva, S. E. Russek, R. Geiss, C. Jones, N. Clark, T. Leo, and D. J. Smith, Phys. Rev. B **80**, 184419 (2009).
[12] J. M. Shaw, S. E. Russek, T. Thomson, M. J. Donahue, B. D. Terris, O. Hellwig, E. Dobisz, and M. L. Schneider, Phys. Rev. B **78**, 024414 (2008).
[13] B. D. Belle, F. Schedin, T. V. Ashworth, P. W. Nutter, E. W. Hill, H. J. Hug, and J. J. Miles, IEEE Trans. Magn. **44**, 3468 (2008).
[14] P. Krone, D. Makarov, T. Schrefl, and M. Albrecht, J. Appl. Phys. **106**, 103913 (2009).
[15] R. Dittrich, G. H. Hu, T. Schrefl, T. Thomson, D. Suess, B. D. Terris, and J. Fidler, J. Appl. Phys. **97**, 10J705 (2005).
[16] G. Hu, T. Thomson, C. T. Rettner, and B. D. Terris, IEEE Trans. Magn. **41**, 3589 (2005).
[17] N. Kikuchi, R. Murillo, J. C. Lodder, K. Mitsuzuka, and I. Shimatsu, IEEE Trans. Magn. **41**, 3613 (2005).
[18] O. Ozatay, T. Hauet, S. H. Florez, J. A. Katine, A. Moser, J. U. Thiele, L. Folks, and B. D. Terris, Appl. Phys. Lett. **95**, 172502 (2009).
[19] O. Hellwig, T. Hauet, T. Thomson, E. Dobisz, J. D. Risner-Jamtgaard, D. Yaney, B. D. Terris, and E. E. Fullerton, Appl. Phys. Lett. **95**, 232505 (2009).
[20] J. E. Davies, O. Hellwig, E. E. Fullerton, G. Denbeaux, J. B. Kortright, and K. Liu, Phys. Rev. B **70**, 224434 (2004).
[21] P. Gaunt, J. Appl. Phys. **59**, 4129 (1986).
[22] N. D. Rizzo, T. J. Silva, and A. B. Kos, Phys. Rev. Lett. **83**, 4876 (1999).
[23] E. D. Dahlberg, D. K. Lottis, R. M. White, M. Matson, and E. Engle, J. Appl. Phys. **76**, 6396 (1994).
[24] R. W. Chantrell, A. Lyberatos, M. Elhilo, and K. Ogrady, J. Appl. Phys. **76**, 6407 (1994).
[25] M. J. Donahue and R. D. McMichael, IEEE Trans. Magn. **43**, 2878 (2007).